Mobile sensors for hydraulic calibration of pipe network models

Alemtsehay G. Seyoum, Simon Tait, Alma N.A. Schellart, Will Shepherd, Joby Boxall
School of Mechanical, Aerospace and Civil Engineering, The University of Sheffield, United Kingdom
Corresponding author: a.g.seyoum@sheffield.ac.uk

Abstract

This paper is the first to explore the potential use of mobile sensors in the hydraulic calibration of water distribution system and sewer system network models. Novel simulation and optimisation functionality is developed to simulate, utilise and analyse the data that would be collected from mobile hydraulic sensors. Comparable functionality is obtained for static sensors to demonstrate the benefits for a mobile sensor approach. Real world case studies are used to show and compare the accuracy of resulting model calibration, with pipe roughness used to independently assess the calibration quality achieved. Mobile sensors achieved substantially lower pipe roughness error values, around 50% lower in the water supply network and around 25% lower in the sewer network. This level of relative predictive performance was demonstrated for 24 hours of data collection from a single mobile sensor, in comparison to nearly 97% nodal coverage of the water supply network and 66% coverage of combined sewer network by static sensors – all sensors sampled at the same frequency. The evidence generated shows the significant potential of mobile sensors, deployed on robotic platforms, to transform the accuracy of water supply and sewer network model calibration. Such improvements are essential to enable, and as part of, digital twin paradigms and to confidently inform proactive management driven from accurate and comprehensive assessment of system performance.

1. Introduction

"All models are wrong, but some are useful" (Box, 1976). Their usefulness depends on how accurately they represent reality and how well they are calibrated. Water supply and sewer network models are typically calibrated using data from a limited number of fixed locations, such as pressure measurements in water supply systems or depth and velocity in sewer systems (Bertrand-Krajewski, 2003; Meirelles et al., 2017). Once there is sufficient confidence in the geometrical representation of reality in the models, parameters like pipe roughness are adjusted to ensure the model simulations align with observed data. These models are then used to evaluate system performance, including maintaining minimum pressure criteria, detecting leaks, managing flood risks, handling combined sewer overflow spills, and enabling real-time control. However, due to their inherent complexity and the under-constrained nature of their solution space, these models can appear accurate for specific predictions while misrepresenting other system behaviours (Walski, 2000; Her and Chaubey, 2015). For example, correct pressure or head losses can be simulated using multiple parameter combinations, which may result in inaccuracies in flow velocity predictions or transport routes (Boxall et al., 2004). This

reliance on limited calibration data often leads to poor predictions of broader system behaviours, such as more extreme hydraulic conditions or water quality dynamics (e.g., water age or chlorine residuals in water supply or Total Suspended Solids (TSS), COD or temperature in sewer systems), particularly when uncertainties linked with reaction/heat transfer coefficients are involved.

This study pioneers a new approach to hydraulic model calibration by introducing the concept of the use of moving (robotic) sensors, marking a departure from conventional static sensor approaches. It evaluates the effectiveness of mobile sensors in improving calibration accuracy within complex systems and benchmarks their performance against (optimised) conventional methods. Through real world case studies in both water supply and combined sewer networks, the study demonstrates the application of this method, aiming to advance calibration practices in large-scale pipe networks subject to dynamic patterns of use and hydraulic loading.

2. Background

2.1. Optimising static sensor placement for hydraulic model calibration

Accurate hydraulic model calibration relies on the availability of reliable data; data used for calibration must be independent of input model data. For water supply systems, District Metered Area (DMA) inflow data and customer demand (where available) are often used as model inputs. For sewer systems, dry weather flow and rainfall data are often used as model inputs. Consequently, pressure in water supply systems and depth and velocity in sewer systems are the primary independent calibration data. These calibration data are typically obtained from static monitors, with increasing numbers of locations and higher sample frequency enhancing data availability and hence model calibration accuracy.

The efficacy and value derived from different numbers and combinations of fixed sensor locations has been the subject of many optimisation studies including hydraulic model calibration (e.g., Kapelan et al., 2003), leak detection and localisation (e.g., Boatwright et al., 2023), early warning systems for sewer overflows (e.g., Do et al., 2023) and blockage detection in sewer systems (e.g., Ninh et al., 2025).

Numerous optimisation techniques have been developed to improve sensor placement in water supply and sewer networks. These include stochastic programming (Shastri & Diwekar, 2006), exact nonlinear formulations with linear approximations for imperfect sensors (Berry et al.,

2009), and heuristic approaches such as greedy algorithms (Zhao et al., 2016). Multi-objective genetic algorithms, such as the Non-Dominated Sorting Genetic Algorithm II (NSGA-II; Deb et al., 2002), have also gained widespread use in this context (Banik et al., 2017; Ferreira et al., 2023). Beyond sensor placement, NSGA-II has proven effective in broader water supply and sewer system optimisation tasks due to its ability to balance trade-offs between competing objectives, maintain solution diversity through crowding distance, and preserve high-quality solutions via its elitist mechanism (e.g., Rathnayaka & Tanyimboh, 2015; Tanyimboh & Seyoum, 2016).

2.2. Challenges and Constraints of Static Sensing Approach

While static sensor networks have contributed to advancing calibration efforts, they have inherent practical limitations. They have to be installed in accessible locations such as manholes or hydrants. Hence, static sensors often leave substantial spatial coverage gaps, particularly in remote or hard-to-reach areas of the network (Mounce et al., 2021), which can limit the accuracy of the calibration process.

Conventionally, static sensors generally provide data at a 15-minute resolution for water supply to capture daily dynamics and a 1- to 5- minute resolution for rainfall induced dynamics in sewer systems (Mounce et al., 2015, Cristiano et al., 2017). This resolution is particularly useful for calibrating models over a longer period, providing better constraints on model dynamics compared to simulations that focus solely on daily average or peak hour conditions. While higher temporal-resolution data from static sensors can aid in event detection (Mounce et al., 2012), its value for improving hydraulic model calibration remains limited.

The integration of networks of static sensors with online modelling, data-driven analysis, real-time control, and digital twins is enhancing system performance and decision-making of water supply and sewer systems. Online modelling and data-driven analysis use real-time and historical data to optimise operations and detect anomalies, mitigating disruptions like mains bursts in water supply systems (Machell et al., 2010; Mounce et al., 2015), and reducing combined sewer overflows and environmental impact in sewer systems (van Daal et al., 2017; Van der Werf et al., 2023). Building on these advancements, digital twins aim to create near real-time models that are representative of actual physical conditions; these require excellent levels of calibration to enable accurate predictive analysis and automated control (VanDerHorn & Mahadevan, 2021). Despite these advances, static sensors still struggle to capture spatial

variability in large networks, emerging technologies such as sensors placed on mobile robotic platforms offer promising solutions to this capability gap.

2.3. Mobile sensor technologies in pipe networks

Mobile sensor technologies, including robotic systems, are emerging for the inspection and monitoring of buried pipelines. Devices such as SmartBall and PipeDiver have been developed to enhance the monitoring of water and wastewater pipelines, addressing key issues like leak detection, structural integrity assessment, and gas pocket identification (Xylem, 2022; Xylem, 2024) or pollutant monitoring in sewer systems (Maruejouls & Sakarovitch, 2021). These devices are designed to move with the flow of water, gathering data primarily of the flow path (Parrott et al., 2020). Simulation studies have also explored the use of mobile sensors for tasks such as contaminant detection and leak localisation (Perelman & Ostfeld, 2013; Gong et al., 2016).

Advances in pervasive autonomous robotics present further opportunities to revolutionise pipe inspection and monitoring. Autonomous robotic devices are being developed and designed to navigate complex, uncertain, harsh environments, such as buried water and sewer pipe networks. Recent research has demonstrated the effectiveness of such autonomous robots in laboratory settings, where they successfully explore and inspect pipe networks (Nguyen et al., 2022). If equipped with suitable sensor(s) and data acquisition and communication, mobile robotic platforms have the potential to collect data in hard-to-reach areas that are inaccessible to traditional static inspection methods (Mounce et al., 2021).

A practical, autonomous robotic platform for water level or pressure monitoring in water supply and sewer systems does not currently exist. To develop such a platform, then two key scientific capabilities are needed; accurate location mapping and safe, autonomous locomotion control for the robotic platform that is carrying the hydraulic sensors. This allows robotic platforms to know where they are exactly in a system and, if their path is blocked, to access the inaccessible part of the system via a different route. The pipebots project (www.pipebots.ac.uk), was a large UK scientifically focussed project that tested the feasibility of using small, autonomous in-pipe robots with sensors to inspect water supply and sewer networks. This project delivered algorithms for accurate location of in-pipe robotic systems and also in-pipe robotic control for safe location in a pipe network (Li X.S. et al. 2023; Nguyen et al., 2022, Edwards et al. 2023). Therefore, the scientific knowledge has been developed but

there are many practical engineering challenges that remain (e.g. power, mechanical robustness). These issues are being considered in more recent projects (e.g EU pipeon (https://pipeon.eu/) and the German KaSyTwin sewer digital twin project see Hartmann et al, 2025). The increasing funding for the later innovation projects provides evidence that autonomous robotic platforms for hydraulic in-pipe measurements are likely to be developed.

2.4. Use of hydraulic pipe roughness to assess the quality of network model calibration

Any model input should be questioned during calibration. But the different input parameters have varying degrees of uncertainty and impact on simulation accuracy associated with them. Demands (in water supply) and runoff and rainfall (in sewers) have a considerable influence on flow simulations (Babayan et al., 2005; Schellart et al., 2012). It is essential that uncertainty and variability in these is understood before focusing on other calibration parameters. Once these are confirmed, accurately calibrating pipe roughness is often the next crucial parameter for enhancing the reliability of hydraulic network simulations. Hydraulic pipe surface roughness often has large uncertainty and significant impact on predictive performance, particularly for rare events so it is a sensitive and key calibration parameter in the modelling of pipe networks. Head loss, a critical factor in hydraulic network modelling, increases with the square of flow velocity, meaning small inaccuracies in pipe hydraulic roughness values can cause significant deviations in predicted flow behaviour. This is particularly important in geometrically complex infrastructure, subject to varying hydraulic conditions where variations in the pipe hydraulic roughness can substantially alter the simulated flow characteristics

3. Multi-objective optimisation frameworks for comparing mobile and static sensing approaches

A new mobile sensor simulator is developed to simulate the movement of mobile sensors through water supply and combined sewer networks, allowing the exploration of their ability to traverse geometrically complex systems and gather data at different frequencies that can be used for hydraulic roughness calibration.

Equivalent multi-objective optimisation frameworks are developed and applied to optimise the calibration of water supply and combined sewer network models using the available pressure and depth, respectively. While sewer system calibration can involve measurements of both depth and velocity (see Section 2), this study uses only depth to maintain consistency with water supply network calibration. The optimisation frameworks are designed and implemented

to enable fair comparison of calibration accuracy between mobile and static sensors. The frameworks have necessary differences; however, in this work the use of computational options that favoured fixed sensors were generally selected. Chief amongst these is that the static sensors framework optimises the numbers and locations of sensors, whilst for mobile sensors, the route and speed are fixed (not optimised).

The time interval is consistent between the static and mobile simulations and is set to ensure that a data sample would always be collected even from the shortest pipe (if it was visited) as a function of the mobile sensor's speed. Internal pipe hydraulic roughness is selected as a key calibration parameter as detailed in Section 2.4 of the background. To ensure robust comparison, the approach uses a post-calibration evaluation of the differences between optimised pipe hydraulic roughness values and (assumed) actual hydraulic roughness for an assessment that is independent of the calibration data. There are multiple parameters, for example mobile sensor pathway and robotic platform speed that could and ultimately should be optimised to obtain the best quality dataset when carrying out roughness calibration using mobile sensors. However, the mobile sensor parameters are intentionally kept fixed to limit computational effort and favour the static calibration optimisation. Four arbitrary routes from randomly selected starting points are studied for each system to show pathway dependence. For water supply and sewer networks the data collection period is restricted to 24 hours, with the storm event used in the combined sewer simulation fully complete within this period. Sensor platform speed was selected such that the mobile sensor could theoretically traverse the entire length of the pipe network twice in the 24 hours, but due to network complexity and repetition in the pathway many pipes remained unvisited. We assume a simple scenario where the mobile sensor moves with a constant speed, independent of the flow magnitude or direction at any given location or time. If the sensor's speed were to be adjusted relative to local flow conditions, additional considerations such as energy use, power harvesting, and locomotion efficiency would need to be considered, which are outside the scope of this study.

The key simulation assumptions for mobile sensors considered in this study are as follows:

- Sensor paths are predefined, based on random routing decisions at junctions, with equal probability among all connected links.
- The sensor travels at a constant speed, independent of the flow magnitude or direction at any location or time.
- Data are collected continuously at fixed time intervals during movement.

- Sensor movement is assumed unconstrained by physical, hydraulic, or operational barriers.

The procedure for mobile sensor simulation and hydraulic data collection in water supply and combined sewer networks is detailed in the flowchart presented in Figure 1. As the sensor moves, it queries the hydraulic model at each sampling time step (Δt) for pressure or depth data. These values are obtained at the sensor's current position by linearly interpolating results from adjacent computational nodes within a single time step. At each time step, the sensor assesses its position relative to computational nodes along its path. After each data collection cycle, the time is updated by Δt, maintaining consistent timing for each data point collected throughout the operation. The sensor continues this process, traversing the network and gathering data until the cumulative time reaches the duration T.

3.1. Description of case study networks

This section describes two distinct network types, a water supply network and a combined sewer network, used to evaluate and compare the calibration performance of static and mobile sensing approaches in terms of accuracy and efficiency. The water supply network case study is an example of an actual UK DMA, including both branched and looped configurations as shown in Figure 2. The network layout depicted in the figure has been obfuscated (anonymised) using the method described by Collins (2023), connectivity information is preserved but pipe lengths and relative nodal locations are distorted for the visual representation. The system comprises 100 nodes and 109 pipes, with a total network length of 10.7 km. For the calibration of this network daily demand profiles at 15 minutes interval at each node were used.

The case study sewer network is based on the open-access network model of the Bellinge combined sewer system in Denmark (Pedersen et al., 2021). A hydraulically isolated gravity-driven portion of the network was abstracted, to be similar to the combined length of pipes in the studied UK water supply network (see above). It consists of 135 sub-catchments, 196 nodes, 202 conduit links, and approximately 10.4 km of pipes. The layout of the sewer network is shown in Figure 3. It is typical of combined sewer networks, dominated by a dendritic layout.

A high-intensity, short-duration rainfall event from the Bellinge dataset was selected to ensure a substantial range of flow and surcharge conditions during the 24-hour simulation period, making it appropriate for assessing the quality of the hydraulic calibration. The rainfall event was from June 7, 2010 (03:27–12:34), recorded at 1- minute frequency, with a peak intensity of 60 mm/hr, a total rainfall volume of 47.6 mm, and a duration of 9.12 hours. The corresponding precipitation time series is shown in Figure 4.

In both case studies, the original calibrated hydraulic models were assumed to represent the "true" system state and were used to generate a consistent baseline of sensor data used in subsequent comparative analysis. All (static or mobile) optimisations were initiated from random (from a plausible range) hydraulic pipe roughness values in all pipes, with no cognisance of the assumed "true" hydraulic roughness values obtained in the baseline scenario.

During the static and mobile sensor optimisation processes, pipe hydraulic roughness values were iteratively adjusted to improve the model calibration. For the water supply network, the Darcy-Weisbach headloss equation is applied:

$$h_f = f \cdot \frac{L}{D} \cdot \frac{v^2}{2g} \tag{1}$$

where h_f is the head loss due to friction (m); f is the friction factor (dimensionless); L is the pipe length (m); D is the diameter (m); v is the flow velocity (m/s); and g = 9.81 m/s^2. The friction factor f for turbulent flow is based on the Colebrook–White equation, with the Swamee–Jain approximation given as:

$$f = 0.25 \left[\log_{10} \left(\frac{k_s}{3.7D} + \frac{5.74}{Re^{0.9}} \right) \right]^{-2} \tag{2}$$

where k_s is the roughness height (m) and Re is Reynolds number. In this work, k_s is ranged from 0.045 to 6.77 mm. This range was obtained from 19 calibrated real network models representing UK DMAs, comprising over 25,500 pipes. These models represent operational networks in the UK and were calibrated according to the standard UK practice. Sixteen roughness classes were derived from the histogram of these pipe roughness data. An equal-area

histogram approach was used to ensure that each class contained a similar proportion of the total data. The midpoint of each class was selected as its representative, forming sixteen candidate roughness values for optimisation.

For the sewer network, the Manning equation is applied:

$$Q = \frac{1}{n} A R^{2/3} S^{1/2} \quad (3)$$

where Q is the flow rate (m3/s), n is the Manning roughness coefficient (dimensionless), A is the cross-sectional flow area (m^2); R is the hydraulic radius (m) and S is the slope of the energy grade line. In this work, roughness values were generated using the log-logistic distribution parameters of the roughness height (k_s) reported by Sriwastava et al. (2018). The distribution parameters were derived from a 10-year flow survey conducted in a single combined sewer network. The resulting k_s values were then converted to Manning's n (ranging from 0.006 to 0.026) using the approximation from Marriott and Jayaratne (2010). Sixteen candidate roughness values were subsequently selected from this range for use in the optimisation of pipe roughness calibration. The complete list of discrete pipe roughness values for both water supply and sewer networks is provided in Table S1 of the Supplementary Material.

The optimisation process for both mobile and static sensing approaches employs the NSGA-II algorithm, as outlined in Section 2.1. The algorithm represents candidate solutions using binary encoding and evolves them through bitwise mutation, single-point crossover, and tournament selection. Each individual in the NSGA-II population represents a candidate set of pipe roughness values, which are iteratively updated during the optimisation process. For the static sensing case, the individual additionally includes the sensor configuration, the numbers and locations of sensors, so that these parameters are optimised together with pipe roughness. At each iteration, all individuals are evaluated using the two objective functions defined in Section 3.2. The best-performing solutions are selected and recombined through crossover and mutation to generate new candidates with updated roughness values. This iterative process continues until the convergence criteria are met.

3.2. Objective function formulations

Two objective functions ($f_1$and f_2) were used to provide comparable results across the static and mobile sensing approaches. The first (f_1) is the commonly used objective to minimise the residuals between baseline and optimised model-predicted sensor values. The values were head differences for water distribution and depth for sewer networks. The second objective function (f_2) is new for hydraulic network model calibration, added to provide a measure of the information quality and coverage - how well the sampled data represents the range of all data - to drive efficiency in the deployment strategy. The function comprises two components: (i) a spatial coverage term**,** defined differently for static and mobile sensing, representing the proportion of the network observed (for fixed sensors, the fraction of monitored nodes; for mobile sensors, the fraction of visited links); and (ii) a variance-based term, which quantifies how closely the variability in the sampled data matches the overall hydraulic variability of the network. This second term is conceptually similar to information-theoretic measures such as mutual information (Crowley et al., 2025). It captures the extent to which sensor data reflects the full dynamic range of system behaviour, ensuring that measurements are not concentrated in hydraulically uniform regions. Together, these components promote informative and spatially distributed sampling, leading to a more representative characterisation of the network's hydraulic state. This objective function drives the optimisation of fixed sensors numbers and locations, and observing this parameter allows us to compare between the 4 different pathways studied for the mobile sensors.

Together, these two objectives balance model accuracy and data richness, guiding a calibration process that is both accurate and efficient for water supply and sewer networks.

3.2.1 Static sensing

The objective functions for static sensing are formulated as follows:

$$\text{Minimise } f_1^{(s)} = \sqrt{\frac{1}{N_s \cdot T}\sum_{t=1}^{T}\sum_{n=1}^{N_s}\left(H_{base}^{s}(t,n) - H_{pred}^{s}(t,n)\right)^2} \quad (4)$$

$$\text{Maximise } f_2^{(s)} = \alpha \cdot \left[1 - \frac{\left|\sigma_s^2 - \sigma_{network}^2\right|}{\sigma_{network}^2}\right] + (1-\alpha) \cdot \left[\frac{N_s}{N}\right] \quad (5)$$

where $f_1^{(s)}$ and $f_2^{(s)}$ represent the first and second objective functions for static sensing. Hereafter, H denotes hydraulic data, representing head in water supply systems and depth in sewer systems. Specifically, $H_{base}^s(t,n)$ and $H_{pred}^s(t,n)$ represent baseline and model-predicted sensor values at time t and static node n. The mean (μ_s) and the variance (σ_s^2) of $H_{pred}^s(t,n)$ are provided as:

$$\mu_s = \frac{1}{T \cdot N_s} \sum_{t=1}^{T} \sum_{n=1}^{N_s} H_{pred}^s(t,n) \quad (6)$$

$$\sigma_s^2 = \frac{1}{T \cdot N_s} \sum_{t=1}^{T} \sum_{n=1}^{N_s} \left(H_{pred}^s(t,n) - \mu_s\right)^2 \quad (7)$$

where N_s is the current total number of static sensor nodes, and T is the total number of time steps.

The mean ($\mu_{network}$) and the variance ($\sigma_{network}^2$) of $H_{pred}(t,n)$ for all nodes and time steps in the network are given by:

$$\mu_{network} = \frac{1}{T \cdot N} \sum_{t=1}^{T} \sum_{n=1}^{N} H_{pred}(t,n) \quad (8)$$

$$\sigma_{network}^2 = \frac{1}{T \cdot N} \sum_{t=1}^{T} \sum_{n=1}^{N} \left(H_{pred}(t,n) - \mu_{network}\right)^2 \quad (9)$$

where N is the total number of nodes in the network.

In Equations (5), α was set to 0.5 to equally balance variance-based information gain and spatial coverage.

3.2.2 Mobile sensing

The objective functions for mobile sensing are defined as follows:

$$\text{Minimise } f_1^{(m)} = \sqrt{\frac{1}{T}\sum_{t=1}^{T}\left(H_{base}^{m}(x(t),y(t),t) - H_{pred}^{m}(x(t),y(t),t)\right)^2} \tag{10}$$

$$\text{Maximise } f_2^{(m)} = \alpha \cdot \left[1 - \frac{\left|\sigma_m^2 - \sigma_{network}^2\right|}{\sigma_{network}^2}\right] + (1-\alpha)\cdot\left[\frac{P_u^m}{P}\right] \tag{11}$$

where f_1^m and f_2^m represent the first and second objective functions for mobile sensing. $H_{base}^{m}(x(t),y(t),t)$ and $H_{pred}^{m}(x(t),y(t),t)$ represent the baseline and model-predicted sensor values, respectively, at time step t, for a mobile sensor at pipe network location $\left(x(t),y(t)\right)$; these values may vary as the sensor moves through the system.

It should be noted that the values of t referenced in Equations (4) and (10) remain identical for evaluating both the static and mobile sensor approaches.

The mean (μ_m) and the variance (σ_m^2) of $H_{pred}^{m}(x(t),y(t),t)$ are provided as:

$$\mu_m = \frac{1}{T}\sum_{t=1}^{T} H_{pred}^{m}(x(t),y(t),t) \tag{12}$$

$$\sigma_m^2 = \frac{1}{T}\sum_{t=1}^{T}\left(H_{pred}^{m}(x(t),y(t),t) - \mu_m\right)^2 \tag{13}$$

where T is the total number of times steps, indicating the total data points collected. The formulation assumes that the mobile sensor collects one measurement per time step at its current location.

In Equation 11, $\sigma^2_{network}$ represents the overall variance of hydraulic data for the entire network, as previously defined in Equation 9 for the static sensing approach. The term P_u^m denotes the number of unique pipes visited by the mobile sensor, while P indicates the total number of pipes in the network. Since the mobile sensor follows a fixed route, the number of unique pipes visited, and thus the spatial coverage ratio $(P_u^m|P)$ remains constant throughout the optimisation process. In contrast, the static sensor coverage ratio $(\mathrm{N_s}|\mathrm{N})$, as used in Equation 5, varies with the number and placement of sensors, enabling the objective function to reward increased spatial coverage during optimisation. This introduces a degree of bias toward the static sensor approach. However, the fixed spatial coverage term $(P_u^m|P)$ is retained in the mobile sensor formulation to maintain a consistent comparison.

In Equations 5 and 11, the second objective functions ($f_2^{(s)}$and $f_2^{(m)}$) for static and mobile sensing aim to maximise information gain by increasing the proportion of variance captured by the current sensor configuration (σ_s^2, σ_m^2) relative to the total network-wide variance ($\sigma^2_{network}$). These variances are dynamically computed at each generation of the optimisation using the pipe roughness values of the candidate solutions being evaluated. This allows the objective function to reflect how well the given sensor configurations capture system behaviour and contribute to accurate model calibration. The $f_2^{(s)}$and $f_2^{(m)}$ values range from 0 to1, where higher values indicate that the sensor data more fully capture network's hydraulic variability.

For both sensing approaches, hydraulic analyses for the optimisation process are performed using EPANET for water supply networks and SWMM for sewer networks, inherently satisfying mass balance and energy conservation constraints. These software packages provide the hydraulic data required to evaluate solution fitness. The autonomous mobile sensor simulation and hydraulic data collection procedure (illustrated in Figure 1) is automatically repeated for each generation in the NSGA-II, with hydraulic roughness values updated automatically in EPANET for water supply systems and SWMM for sewer systems.

3.3. Sensor deployment and optimisation setup

In the static sensing approach, all network nodes were evaluated as potential sensor locations. Each static sensor in the water supply network collected pressure data over a 24-hour period at a 3-minute interval (480 samples), matching the mobile sensor's sampling rate. It should be noted that the input demand data has a resolution of 15 minutes and the extended period

simulation in EPANET is not dynamic, so the fixed sensor data will return repeat values as will the mobile (subject to interpolation along the pipe) unless the sensor moves to a new pipe or the simulation advances to a new demand time step. The logic of how static and mobile sensors record pressure data within EPANET's extended-period simulation is provided in Supplementary Figure S1. Similarly, in the sewer network, each static sensor recorded depth data at a 10-second interval (8,640 samples) over 24 hours, ensuring consistency with the mobile sensor. It should also be noted that the rainfall input data has a resolution of 1 minute. Since this is a dynamic simulation that accounts for backwater effects and other unsteady flow conditions, changes in hydraulic values in the sewer system can be observed at this temporal resolution for both mobile and static sensors.

To assess mobile sensing performance, four randomly selected paths each starting from different initial deployment nodes were chosen. The mobile sensor's movement was modelled as a random walk based on the network topology. Specifically, the path generation procedure began by randomly selecting an initial deployment node. At each junction, the next link was chosen at random with equal probability among all connected links, excluding the link just traversed, to avoid immediate backtracking. The movement continued for a 24-hour simulation period. These four independently generated paths, each with different starting nodes and link sequences, were used for calibration in both the water supply and sewer networks.

Figure 5 shows the obfuscated starting locations and water supply network paths. Figure 6 shows the starting locations and sewer network paths. In the water supply network, pressure data was collected every 3 minutes ensuring the possibility of collecting at least one measurement per pipe even in the shortest pipe (48 m). In the sewer network, depth data was recorded every 10 seconds. On average, the proportion of unique pipes visited by the mobile sensor, relative to the total number of pipes in the network, was approximately 83% (range: 80%-84%) for the water supply network and 56% (range: 48%-63%) for the sewer network, for the different sensor pathways. This indicates that the sensor visited several pipes multiple times, capturing data on varying hydraulic conditions at different times throughout the network due to the time varying nature of the flows in each network type.

For static sensing, five optimisation runs were performed for both the water supply and sewer networks. Each run was initialised with a different randomly generated population comprising

encoded strings representing pipe roughness values and sensor placement configurations including both the numbers and locations of sensors.

For mobile sensing in the water supply network, five random optimisation runs were performed for each sensor pathway, with a single sensor deployed in each run, resulting in a total of 20 runs. Each run was initialised with a randomly generated population comprising encoded strings that represent pipe roughness values, with the sensor pathway and speed fixed per set of runs. Similarly, in the sewer network, five runs were conducted per sensor pathway under the same conditions, also totalling 20 optimisation runs.

In both static and mobile sensing scenarios, the crossover and mutation probabilities were set to 1.0 and 0.005, respectively. For the water supply network, the optimisation process was executed for 5,000 generations with a population size of 400, resulting in 2,000,000 function evaluations per run. For the combined sewer network, the process was conducted for 5,000 generations with a population size of 200, leading to 1,000,000 function evaluations per run. Adapting the methodology of Trautmann et al. (2008), who assessed Pareto front stability using performance indicators over a generational window, we define the convergence generation for each objective as the earliest generation at which its absolute change over a 50-generation span remains below 10^{-4} for all subsequent generations. The solution convergence generation is the maximum of the two objectives' convergence generations, which allows both objectives to reach stability. A summary of the key simulation and optimisation parameters used in this study, including their values, sensing types, applicable scenarios (water supply and sewer networks), and the rationale for their selection, is provided in Table S2 of the Supplementary Material.

We evaluated the effectiveness of both static and mobile sensing approaches by assessing the mode (i.e., the most frequent value) of the absolute hydraulic pipe roughness errors across the network, thus independent of data used in the optimisation. The original network pipe roughness values served as the 'ground truth' for comparison. The mode was chosen as a key metric because pipe roughness errors exhibit a skewed distribution, with a few pipes having relatively much larger roughness errors. Using the mode helps reduce the impact of extreme values and provides a representative measure of estimation accuracy.

4. Results

4.1 Water supply network

4.1.1 Optimisation progress for static and mobile sensing in the water supply network

Figure 7 presents the optimisation progress of the two objective functions: residual head (f_1^s for static sensing and f_1^m for mobile sensing), defined in Equations (4) and (10), and information quality and coverage (f_2^s and f_2^m), defined in Equations (5) and (11). The values represent the best-performing individuals for each objective at every generation. These best values are typically obtained from different individuals in the population, as NSGA-II maintains a diverse population and optimises each objective independently during the search process. For mobile sensing, the example of the results shown in the graphs correspond to the sensor path originated at the peripheral node (N1) in the water supply system. While all four paths were analysed, only this path is shown in the graphs for brevity. Subfigures (a) and (b) use a logarithmic scale on the y-axis to enhance visual clarity. In both cases, the optimisation trajectories for static and mobile sensing show a steep initial decrease in residual head (f_1^s and f_1^m), followed by a more gradual decline over the subsequent generations. Table 1 provides details on the objective function values and their corresponding convergence generations for both static and mobile sensing approaches. On average (5 runs), static sensing converges to f_1^s = 0.7 x 10^{-3} m at generation 456, while mobile sensing along Path N1 converges to f_1^m = 1.7 x 10^{-3} m at generation 272. The table again shows the sensitivity of the solution to the pathway. The best performing mobile sensing path is N87, achieving f_1^m = 0.4 x 10^{-3} m at generation 79. Considering all four mobile sensing paths (20 runs in total), the overall average convergence for mobile sensing is f_1^m = 1.6 x 10^{-3} m at generation 227. Subfigures (c) and (d) illustrate the corresponding progression of information coverage (f_2^s and f_2^m). The optimisation trajectories for static sensing exhibit a steep initial increase, which flattens within the first few thousand generations. In contrast, the trajectories for mobile sensing show minimal variation across generations. This is expected, as we do not optimise any aspect of the mobile sensor coverage due to its fixed path and speed. For static sensing, the average convergence (5 runs) reaches f_2^s= 0.995 at generation 1010, while for mobile sensing, the average of all the 20 runs (covering all four sensor paths) converges to f_2^m = 0.907 at generation 173**.** On average, the solution converged at generation 1203 for static sensing and 292 for mobile sensing.

The lower f_2^m values in mobile sensing are attributed to the fixed path and speed settings used in this study, which limit spatial coverage compared to the optimised fixed-sensor placement.

Table 1. Objective function values and convergence generations for static and mobile sensing in the water supply network.

Sensing type	Sensor path	f_1^*(m)	f_2^*	f_1^* convergence generation	f_2^* convergence generation	Solution convergence generation
Static						
Run 1	_	0.7 x 10^{-3}	0.995	91	873	873
Run 2	_	0.8 x 10^{-3}	0.995	83	1369	1369
Run 3	_	0.8 x 10^{-3}	0.995	1758	792	1758
Run 4	_	0.5 x 10^{-3}	0.995	251	682	682
Run 5	_	0.8 x 10^{-3}	0.995	97	1332	1332
Average (Static)		**0.7 x 10^{-3}**	**0.995**	**456**	**1010**	**1203**
Mobile	Path N1	1.7 x 10^{-3}	0.888	272	532	532
	Path N24	1.1 x 10^{-3}	0.917	340	53	340
	Path N69	3.1 x 10^{-3}	0.899	217	52	217
	Path N87	0.4 x 10^{-3}	0.922	79	54	79
Average (Mobile)**		**1.6 x 10^{-3}**	**0.907**	**227**	**173**	**292**

*f_1 and f_2 are the two objective functions used in the optimisation, representing f_1^s and f_2^s for static sensing and f_1^m and f_2^m for mobile sensing.

**Mobile results are averaged per pathway (5 runs each), with the overall average based on all 20 runs.

***The solution convergence generation is the maximum of the f_1 and f_2 convergence generations, which allows both to reach stability.

4.1.2 Pareto fronts for static and mobile sensing in the water supply network

Figure 8 presents the Pareto fronts for static and mobile sensing approaches, showing trade-offs between residual head and information coverage. Different axis scales are used in each subfigure to enhance visibility of the respective spreads. For static sensing, f_1^s ranges from 0.1 x 10^{-3} to 2.0 x 10^{-3} m and f_2^s from 0.941 to 0.995, while mobile sensing exhibits a broader f_1^m range (2.0 x 10^{-3} to 1.2 x 10^{-2} m) and a narrower f_2^m range (0.869 to 0.889).

Static sensing involves simultaneous optimisation of the numbers of sensors, sensor locations, and pipe roughness. This increases the dimensionality of the decision space and produces a wider range of trade-off configurations between f_1 and f_2. Consequently, Pareto fronts from different runs are more dispersed and display clearer inflection points. Such flexibility allows

exploration of a broader range of compromise solutions but introduces higher variability across runs. In contrast, for the mobile sensing configuration, the Pareto fronts obtained from multiple optimisations runs appear smoother and more closely aligned. This behaviour results from the constrained search space: the sensor path and speed are predefined, so only the pipe roughness values are adjusted during optimisation. As a result, the trade-off space between f_1 (head residual) and f_2 (information coverage) is narrow, producing more consistent and stable Pareto fronts across runs. From an engineering perspective, the narrower, more aligned Pareto fronts of mobile sensing indicate stable and repeatable calibration performance, valuable for automated or real-time applications. Static sensing achieves higher f_2 (better information coverage) but requires more sensors, whereas mobile sensing maintains a moderate f_2 with a single sensor.

4.2 Sewer network

4.2.1 Optimisation progress for static and mobile Sensing in the sewer network

Figure 9 shows the progression of the two objective functions, residual depth and information coverage, for the best-performing individuals at each generation in the sewer network. The example of the results presented for mobile sensing correspond to sensor path N638, which starts near the outfalls in the sewer system. Only this path is graphed, as other paths showed similar trends. Static sensing runs exhibit relatively greater dispersion in their objective function trajectories, whereas mobile sensing runs demonstrate more consistent performance. In subfigures (a) and (b), both static and mobile sensing show a steep initial reduction in residual depth (f_1^s and f_1^m), followed by a more gradual decline over subsequent generations until convergence. Table 2 provides details on the objective function values and convergence generations for both static and mobile sensing approaches. On average (5 runs), static sensing converges to f_1^s = 3.8 x 10^{-2} m at generation 4609, while mobile sensing along Path N638 converges to f_1^m = 2.3 x 10^{-2} m at generation 3902. An evaluation of the progression of information coverage (f_2^s and f_2^m) is shown in subfigures (c) and (d). The static sensing runs show a steep initial rise but require more generations to converge. In contrast, the trajectories for mobile sensing show minimal variation across generations, as observed in the water supply network. On average (5 runs), static sensing converges to f_2^s = 0.857 at generation 3614, whereas mobile sensing along Path N638, its best-performing path achieves f_2^m = 0.874 at generation 54, outperforming static sensing in both objectives. The range of f_1 (in particular) and f_2 values shown in Table 2 highlight the path-dependent nature of mobile sensing

performance. When considering all four mobile sensing paths (20 runs in total), the overall average convergence is f_1^m= 3.5 x 10^{-2} m at generation 3679 and f_2^m = 0.837 at generation 56. On average, the solution converged at generation 4683 for static sensing and 3679 for mobile sensing.

Compared to static sensing, mobile sensing generally achieves lower residual depth but slightly reduced average information coverage.

Table 2. Objective function values and convergence generations for static and mobile sensing approaches in the sewer network.

Sensing type	Sensor path	f_1^*(m)	f_2^*	f_1^* convergence generation	f_2^* convergence generation	Solution convergence generation
Static						
Run 1	_	3.8 x 10^{-2}	0.854	3859	4231	4231
Run 2	_	3.3 x 10^{-2}	0.869	4998	4518	4998
Run 3	_	3.1 x 10^{-2}	0.853	4732	1032	4732
Run 4	_	4.9 x 10^{-2}	0.862	4680	4597	4680
Run 5	_	3.8 x 10^{-2}	0.849	4774	3692	4774
Average Static		**3.8 x 10^{-2}**	**0.857**	**4609**	**3614**	**4683**
Mobile	Path N110	5.4 x 10^{-2}	0.812	3748	56	3748
	Path N131	3.4 x 10^{-2}	0.834	4480	56	4480
	Path N163	3.0 x 10^{-2}	0.827	2584	57	2584
	Path N638	2.3 x 10^{-2}	0.874	3902	54	3902
Average (Mobile)**		**3.5 x 10^{-2}**	**0.837**	**3679**	**56**	**3679**

f_1 and f_2 are the two objective functions used in the optimisation, representing f_1^s and f_2^s for static sensing and f_1^m and f_2^m for mobile sensing.

***Mobile results are averaged per pathway (5 runs each), with the overall average based on all 20 runs.*

4.2.2 Pareto fronts for static and mobile sensing in the sewer network

Figure 10 presents the Pareto fronts for static and mobile sensing approaches for the 200 members of the final generation, showing trade-offs between residual depth (f_1) and information coverage (f_2). For static sensing, f_1^s ranges from 3.1 x 10^{-2} to 8.3 x 10^{-2} m and f_2^s from 0.720 to 0.869. In contrast, mobile sensing exhibits a broader f_1^m range (2.1 x 10^{-2} to 1.7

x 10^{-1} m) and a narrower f_2^m range (0.834 to 0.874). As observed in water supply network, the Pareto fronts obtained from static sensing are more dispersed within the independent runs. Mobile sensing fronts, on the other hand, are closely aligned, reflecting consistent performance within the runs. Notably, the mobile sensing fronts display well-defined inflection points, indicating optimal trade-off points where low residual depths are achieved with only marginal reductions in information coverage.

4.3 Assessment of static and mobile sensing for network hydraulic roughness calibration using optimisation of the independent pipe roughness error

The aim of the paper was to investigate the performance of mobile and static sensing approaches for network hydraulic roughness calibration. This is evaluated, as outlined in Section 3.3, using the average of the modes of the absolute pipe roughness errors from the final population at generation 5,000. Specifically, the last 400 Pareto front solutions are considered for the water supply network and the last 200 for the sewer network. The results for both sensing approaches are summarised in Table 3. For the water supply network, static sensing yields an average mode pipe roughness error of 1.676 mm across the five runs, while mobile sensing achieves a lower average mode of 0.909 mm over 20 runs. This indicates improved hydraulic roughness calibration accuracy with mobile sensing, corresponding to an average reduction of 46% in pipe roughness error compared to static sensing. Remarkably, the best-performing mobile sensor path, Path N87, attains an average mode roughness error of 0.00 mm.

In the sewer network, the average mode of pipe roughness error from five static sensing runs is 0.004, while mobile sensing yields a lower average of 0.003 based on 20 runs. The best performance among mobile configurations is observed for Path N638, with an error of 0.002. Overall, mobile sensing outperforms static sensing, yielding pipe roughness errors that are 25% lower on average.

Mobile sensing minimised pipe roughness error better, showing higher calibration accuracy for both water supply and sewer networks. This was achieved with one mobile sensor per system. In contrast, static sensing required an average of 97 sensors for the water supply network and 130 for the sewer network.

Table 3. Average mode of absolute pipe roughness error for Pareto front solutions using static and mobile sensing approaches.

Network	Sensing type	Sensor path	Average per run					Average per sensing type
			Run1	Run2	Run3 (mm)*	Run4	Run5	
Water Supply	Static	-	2.650	1.965	1.631	0.000	2.136	**1.676****
	Mobile	Path N1	0.585	0.834	3.119	3.119	3.088	2.149
		Path N24	0.000	0.081	0.000	0.000	0.000	0.016
		Path N69	0.297	2.911	0.000	0.532	3.605	1.469
		Path N87	0.000	0.000	0.000	0.000	0.000	0.000
	Overall Average (Mobile)							**0.909****
Sewer					(--)*			
	Static	-	0.001	0.005	0.002	0.006	0.005	**0.004****
	Mobile	Path N110	0.004	0.003	0.005	0.005	0.004	0.004
		Path N131	0.005	0.002	0.003	0.002	0.002	0.003
		Path N163	0.003	0.003	0.002	0.003	0.005	0.003
		Path N638	0.002	0.002	0.004	0.002	0.002	0.002
	Overall Average (Mobile)							**0.003****

*Roughness height (K_s) is in mm for water supply networks and Manning's n (dimensionless) for sewer networks.

**The overall average for static sensing is based on 5 runs, while for mobile sensing it is based on all 20 runs (5 runs per path for 4 paths).

5. Discussion

The simulations conducted here show that mobile sensing could substantially improve hydraulic roughness model calibration accuracy, achieving an average reduction in pipe roughness error of around 50% in the water supply network and around 25% in the sewer network compared to calibrations based on data from static sensors. Remarkably, in our study this performance was demonstrated using a single mobile sensor restricted to four predefined paths, each tested independently at a fixed speed, without any attempt to optimise the route or speed settings. In contrast, the static sensing approach required an average of 97 (97% of network nodes) sensors in the water supply network and 130 (66% of network nodes) in the sewer network. These results show the potential efficiency and effectiveness of a mobile sensing approach for hydraulic network model calibration. The dependence of mobile sensing calibration on path (Table 3) implies that future research should investigate the optimisation of sensor routes and speeds to improve calibration results. The influence of sensor speed was not examined in this study.

While static sensing yielded lower average nodal head residuals (f_1) in the water supply network, mobile sensing delivered more accurate pipe roughness estimates on average. This is an important advantage when trying to achieve the most physically accurate network model that will perform better over a wider range of hydraulic conditions. Pipe roughness is the key physical variable as it allows the user to obtain better hydraulic simulations for a wider range of hydraulic conditions. It is the accurate calibration of pipe roughness, rather than the minimisation of the objective function f_1 that ultimately supports the development of a true digital twin of the network. The lower head residual (f_1) observed when using static sensors arises from how f_1 is computed. In the static-sensor case, f_1 is calculated across all fixed sensor nodes, including some that may not be particularly informative for roughness calibration. As a result, the average f_1 can appear lower even though the corresponding roughness estimates are less accurate. In contrast, the mobile sensor computes f_1 only along its measurement path, which tends to include hydraulically important nodes, where head is more sensitive to roughness variations, as it traverses multiple parts of the network during the 24-hour simulation. Consequently, f_1 may appear higher because it samples critical nodes, yet it achieves better roughness estimation. This underlines the importance of incorporating independent calibration metrics, such as pipe roughness error, rather than only considering optimisation objectives like f_1 when evaluating and comparing different sensing approaches.

To improve and better inform the sensor deployment strategies and calibration accuracy, this study introduced a new second objective function (f_2), aimed at maximising information quality and coverage. Instead of relying solely on a measure of spatial sensor deployment, f_2 provides a measure of how well the sampled data captures the overall variability of system behaviour. This encourages better targeted sensor placement, both spatially and temporally, focusing on areas where hydraulic conditions vary most, that is those locations that provide the highest quality information for pipe roughness calibration. For network operators, this could promote a shift from exhaustive spatial coverage using large number of static sensors to more strategic data collection, potentially increasing significantly the value of each observation. In this study the weight of the two parts of f_2 was equal (alpha = 0.5), this could be varied in future to fine tune the desired optimisation balance.

The mobile sensor simulations undertaken assumed a speed of travel of 0.25 m/s. This is probably excessive for the automation and power requirements of robots currently being developed. However, it was useful to provide meaningful comparison in the amount of data collected relative to the static sensors. This speed was necessary as a key part of the comparison was to maintain a 24-hour period for all simulations. A robot travelling at a lower speed but for more days is entirely realistic from a mechatronics perspective. Such a robot could achieve the same network coverage as studied here. But with potentially far greater temporal richness, it would increase the value of information captured. The configuration was biased to favour the static approach, but the results show better network calibration performance from mobile sensing even with this biased comparison.

Network topology may influence roughness calibration through its control of hydraulic variability and flow connectivity. In looped systems, interconnected flow paths could create hydraulic redundancy, leading to more uniform head losses and reduced sensitivity to local roughness variations. This redundancy could also mask compensating errors, where inaccuracies in one pipe's roughness are offset by opposing errors along alternative routes. In contrast, branched (dendritic) systems may exhibit stronger flow directionality and greater variation in hydraulic gradients, making them more informative for calibration. The proposed mobile-sensing calibration approach consistently outperformed static sensing in both configurations, indicating robustness to network structure. The branched sewer network exhibited better calibration performance.

In this study, simulations have been constrained to only consider the collection of pressure or depth data, to maintain consistency with what is done currently with static sensors. Mobile robotic sensors have the potential to expand the scope of data collected. Flowrate or velocity data could be more readily collected by mobile sensors, as a single more complex sensor could travel around the network rather than deploying numerous complex sensors at many locations. Such more complex hydraulic data is well known to be valuable for model calibration, provided it is independent of any such data used in any model build. The capital, maintenance and installation costs for flowrate and velocity measurements make it impractical to install such instrumentation in many static locations. However, the instrumentation would only be required once for the single robotic mobile sensor simulated here, and their maintenance costs would be minimal assuming that the robotic sensors are designed for deployment and retrieval via manholes or fire hydrants. The mobility and flexibility of robotic sensors would also enable targeted flowrate or velocity data collection at hydraulically critical locations through further path optimisation. Integrating such valuable data would further enhance network calibration accuracy, particularly for flow-sensitive parameters such as pipe roughness and demand patterns. These concepts could also be extended to water quality consideration, for example turbidity sensing for discolouration modelling or particulate linked organic loading or chlorine measurement for disinfection residuals or temperature sensors to assess and model heat recovery potential.

6. Conclusions

This study demonstrated that data from mobile sensing can substantially improve hydraulic network model calibration accuracy compared to data obtained from static sensing. When applied to both water supply and combined sewer networks using equivalent multi-objective optimisation frameworks, mobile sensing reduced pipe roughness estimation error by approximately 50% and 25%**,** respectively. These outcomes were achieved using a single mobile sensor, evaluated independently along four predefined paths at a fixed speed, with no optimisation of route or speed. The comparative static sensors were placed in 97% and 66% of the nodes in the respective water supply and sewer networks. Despite these conditions, mobile sensing outperformed static approaches. This demonstrates that mobile sensing can deliver more accurate pipe roughness calibration using substantially fewer sensing resources. As such, this evidence presents a compelling alternative to the emerging practice of deploying very large numbers of static sensors in water supply and sewer networks. This study has meaningful

implications for how utilities monitor, calibrate, and manage complex water supply and sewer systems.

Acknowledgement

This work is supported by the UK's Engineering and Physical Sciences Research Council (EPSRC) Programme Grant EP/S016813/1; the Collaborative Urban Drainage research labs communities - Co-UDlabs Project, which received funding from the European Union's Horizon 2020 research and innovation programme under Grant Agreement No. 101008626; and the PipeOn project which received funding from the European Union's Horizon Europe Research and Innovation Programme under Grant Agreement No. 101189847.

719 **References**

720 Babayan, A., Kapelan, Z., Savic, D., & Walters, G. (2005). Least-cost design of water
721 distribution networks under demand uncertainty. *Journal of Water Resources Planning*
722 *and Management*, *131*(5), 375-382.

723 Banik, B. K., Alfonso, L., Di Cristo, C., Leopardi, A., & Mynett, A. (2017). Evaluation of
724 different formulations to optimally locate sensors in sewer systems. *Journal of Water*
725 *Resources Planning and Management*, *143*(7), 04017026.

726 Berry, J., Carr, R. D., Hart, W. E., Leung, V. J., Phillips, C. A., & Watson, J. P. (2009). Designing
727 contamination warning systems for municipal water networks using imperfect
728 sensors. *Journal of Water Resources Planning and Management*, *135*(4), 253-263.

729 Bertrand-Krajewski, J. L., Bardin, J. P., Mourad, M., & Béranger, Y. (2003). Accounting for
730 sensor calibration, data validation, measurement and sampling uncertainties in
731 monitoring urban drainage systems. *Water Science & Technology*, *47*(2), 95-102.

732 Boatwright, S., Mounce, S., Romano, M., & Boxall, J. (2023). Integrated sensor placement and
733 leak localization using geospatial genetic algorithms. *Journal of Water Resources*
734 *Planning and Management*, *149*(9), 04023040.

735 Box, G. E. (1976). Science and statistics. *Journal of the American Statistical*
736 *Association*, *71*(356), 791-799.

737 Boxall, J. B., Saul, A. J., & Skipworth, P. J. (2004). Modeling for hydraulic capacity. *Journal-*
738 *American Water Works Association*, *96*(4), 161-169.

739 Collins, R. (2023). Network Anonymisation Report. The University of Sheffield.
740 Report. https://doi.org/10.15131/shef.data.21644384.v1

741 Cristiano, E., ten Veldhuis, M. C., & Van De Giesen, N. (2017). Spatial and temporal
742 variability of rainfall and their effects on hydrological response in urban areas–a
743 review. *Hydrology and Earth System Sciences*, *21*(7), 3859-3878.

744 Crowley, G., Tait, S., Panoutsos, G., Speight, V., & Esnaola, I. (2025). Information-theoretic
745 sensor placement for large sewer networks. *Water Research*, *268*, 122718.

746 Deb, K., Pratap, A., Agarwal, S.and Meyarivan, T. A. M. T. (2002). A fast and elitist
747 multiobjective genetic algorithm: NSGA-II. *IEEE transactions on evolutionary*
748 *computation*, **6**(2), 182-197.

749 Do, N. C., Dix, L., Lambert, M. F., & Stephens, M. L. (2023). Proactive detection of wastewater
750 overflows for smart sanitary sewer systems: Case study in South Australia. *Journal of*
751 *Water Resources Planning and Management*, *149*(1), 05022016.

752 Edwards, S., Zhang, R., Worley, R., Mihaylova, L., Aitken, J., & Anderson, S. R. (2023). A

753 robust method for approximate visual robot localization in feature-sparse sewer
754 pipes. *Frontiers in Robotics and AI*, *10*, 1150508.
755 Ferreira, B., Antunes, A., Carriço, N., & Covas, D. (2023). NSGA-II parameterization for the
756 optimal pressure sensor location in water distribution networks. *Urban Water*
757 *Journal*, *20*(6), 738-750.
758 Gong, W., Suresh, M. A., Smith, L., Ostfeld, A., Stoleru, R., Rasekh, A., & Banks, M. K.
759 (2016). Mobile sensor networks for optimal leak and backflow detection and localization
760 in municipal water networks. *Environmental modelling & software*, *80*, 306-321.
761 Hartmann, S., Valles, R., Schmitt, A., Al-Zuriqat, T., Dragos, K., Gölzhäuser, P., ... &
762 Smarsly, K. (2025). Digital-Twin-Based Management of Sewer Systems: Research
763 Strategy for the KaSyTwin Project. Water, 17(3), 299.
764 Her, Y., & Chaubey, I. (2015). Impact of the numbers of observations and calibration
765 parameters on equifinality, model performance, and output and parameter
766 uncertainty. *Hydrological Processes*, *29*(19), 4220-4237.
767 Kapelan, Z. S., Savic, D. A., & Walters, G. A. (2003). Multiobjective sampling design for
768 water distribution model calibration. *Journal of Water Resources Planning and*
769 *Management*, *129*(6), 466-479.
770 Li, X. S., Nguyen, T. L., Cohn, A. G., Dogar, M., & Cohen, N. (2023). Real-time robot
771 topological localization and mapping with limited visual sampling in simulated buried
772 pipe networks. Frontiers in Robotics and AI, 10, 1202568.
773 Machell, J., Mounce, S. R., & Boxall, J. B. (2010). Online modelling of water distribution
774 systems: a UK case study. *Drinking Water Engineering and Science*, *3*(1), 21-27.
775 Marriott, M., & Jayaratne, R. (2010). Hydraulic roughness–links between Manning's
776 coefficient, Nikuradse's equivalent sand roughness and bed grain size. *Advances in*
777 *Computing and Technology 2010*, 27-32.
778 Maruejouls, T., & Sakarovitch, C. (2021). *SewerBall: A new concept to inspect sewers using*
779 *mobile wastewater quality sensors.* Paper presented at the 15th International Conference
780 on Urban Drainage, Melbourne, Australia.
781 Meirelles, G., Manzi, D., Brentan, B., Goulart, T., & Luvizotto, E. (2017). Calibration model
782 for water distribution network using pressures estimated by artificial neural
783 networks. *Water Resources Management*, *31*, 4339-4351.
784 Mounce, S. R., Gaffney, J. W., Boult, S., & Boxall, J. B. (2015). Automated data-driven

approaches to evaluating and interpreting water quality time series data from water distribution systems. *Journal of Water Resources Planning and Management*, *141*(11), 04015026.

Mounce, S. R., Mounce, R. B., & Boxall, J. B. (2012). Identifying sampling interval for event detection in water distribution networks. *Journal of Water Resources Planning and Management*, *138*(2), 187-191.

Mounce, S. R., Shepherd, W. J., Boxall, J. B., Horoshenkov, K. V., & Boyle, J. H. (2021). Autonomous robotics for water and sewer networks. *IAHR Hydrolink*, *2*, 55-62.

Nguyen, T. L., Blight, A., Pickering, A., Jackson-Mills, G., Barber, A. R., Boyle, J. H., ... & Cohen, N. (2022). Autonomous control for miniaturized mobile robots in unknown pipe networks. *Frontiers in Robotics and AI*, *9*, 997415.

Ninh, T. H. D., Do, N. C., Zeng, W., & Lambert, M. F. (2025). Optimal Sensor Placement in Smart Sewer Systems Using Network Topology and Elevation. *Journal of Water Resources Planning and Management*, *151*(7), 04025016.

Parrott, C., Dodd, T. J., Boxall, J., & Horoshenkov, K. (2020). Simulation of the behavior of biologically-inspired swarm robots for the autonomous inspection of buried pipes. *Tunnelling and Underground Space Technology*, *101*, 103356.

Pedersen, A. N., Pedersen, J. W., Vigueras-Rodriguez, A., Brink-Kjær, A., Borup, M., & Mikkelsen, P. S. (2021). *Dataset for Bellinge: An urban drainage case study*, Tech. Univ. Denmark [data set], https://doi.org/10.11583/DTU.c.5029124

Perelman, L., & Ostfeld, A. (2013). Operation of remote mobile sensors for security of drinking water distribution systems. *Water research*, *47*(13), 4217-4226.

Rathnayake, U. S., & Tanyimboh, T. T. (2015). Evolutionary multi-objective optimal control of combined sewer overflows. *Water Resources Management*, *29*, 2715-2731.

Schellart, A. N. A., Shepherd, W. J., & Saul, A. J. (2012). Influence of rainfall estimation error and spatial variability on sewer flow prediction at a small urban scale. *Advances in Water Resources*, *45*, 65-75.

Shastri, Y., & Diwekar, U. (2006). Sensor placement in water networks: A stochastic programming approach. *Journal of water resources planning and management*, *132*(3), 192-203.

Sriwastava, A. K., Tait, S., Schellart, A., Kroll, S., Dorpe, M. V., Assel, J. V., & Shucksmith, J. (2018). Quantifying uncertainty in simulation of sewer overflow volume. *Journal of Environmental Engineering*, *144*(7), 04018050.

Tanyimboh, T. T., & Seyoum, A. G. (2016). Multiobjective evolutionary optimization of water

distribution systems: Exploiting diversity with infeasible solutions. *Journal of environmental management*, 183, 133-141.

Trautmann, H., Wagner, T., Naujoks, B., Preuss, M., & Mehnen, J. (2009). Statistical methods for convergence detection of multi-objective evolutionary algorithms. *Evolutionary computation*, *17*(4), 493-509.

van Daal, P., Gruber, G., Langeveld, J., Muschalla, D., & Clemens, F. (2017). Performance evaluation of real time control in urban wastewater systems in practice: Review and perspective. *Environmental Modelling & Software*, *95*, 90-101.

Van der Werf, J. A., Kapelan, Z., & Langeveld, J. (2023). Real-time control of combined sewer systems: Risks associated with uncertainties. *Journal of Hydrology*, *617*, 128900.

VanDerHorn, E., & Mahadevan, S. (2021). Digital Twin: Generalization, characterization and implementation. *Decision support systems*, *145*, 113524.

Walski, T. M. (2000). Model calibration data: the good, the bad, and the useless. *Journal-American Water Works Association*, *92*(1), 94-99.

Xylem. (2022). *SmartBall® condition assessment platform* [PDF]. Xylem. https://www.xylem.com/siteassets/brand/pure-technologies/resources/brochure/pure-technologies-smartball-brochure-q3-2022.pdf

Xylem. (2024). *PipeDiver® condition assessment platform* [PDF]. Xylem. https://www.xylem.com/siteassets/brand/pure-technologies/resources/brochure/pure-technologies-pipediver-brochure.pdf

Zhao, Y., Schwartz, R., Salomons, E., Ostfeld, A., & Poor, H. V. (2016). New formulation and optimization methods for water sensor placement. *Environmental Modelling & Software*, *76*, 128-136.

Figure Captions

Figure 1. Flowchart of the mobile sensor simulation and hydraulic data collection process. The simulation is executed at each generation of the multi-objective optimisation.

Figure 2. Anonymised Water Supply Network layout for a DMA in the UK.

Figure 3. Sewer Network Layout based on Pedersen et al. (2021).

Figure 4. Rainfall intensity versus time plot for the June 7, 2010, event.

Figure 5. Randomly generated fixed mobile sensor paths originating from four different initial deployment nodes in the water supply network.

Figure 6. Randomly generated fixed mobile sensor paths originating from four different initial deployment nodes in the sewer network.

Figure 7. Progression of the residual head (f_1^s and f_1^m) and information coverage (f_2^s and f_2^m) for static and mobile sensing in the water supply network. (a)Progression of f_1^s for static sensing, (b) Progression of f_1^m for mobile sensing path from Node 1, (c) Progression of f_2^s for static sensing, (d) Progression of f_2^m for mobile sensing path from Node 1

Figure 8. Pareto fronts of the non-dominated solutions at the final generation for the water supply network. Note the Y-axes are not in the same scale. (a) Static sensing, (b) Mobile sensing along Path N1.

Figure 9. Progression of the residual depth (f_1^s and f_1^m) and information coverage (f_2^s and f_2^m) for static and mobile sensing in the sewer network. (a) Progression of f_1^s for static sensing, (b) Progression of f_1^m for mobile sensing path from Node 638, (c) Progression of f_2^s for static sensing, (d) Progression of f_2^m for mobile sensing path from Node 638.

Figure 10. Pareto fronts of the non-dominated solutions at the final generation for the sewer network. (a) Static sensing, (b) Mobile sensing along Path N638.

Mobile sensors for hydraulic calibration of pipe network models

Highlights

- First study to explore mobile sensors for calibration of 1D hydraulic models
- Novel mobile-sensing simulation and objective for information quality and coverage
- Mobile sensing substantially improves calibration accuracy compared to static sensing
- More accurate pipe roughness calibration using fewer mobile sensing resources

Graphical Abstract

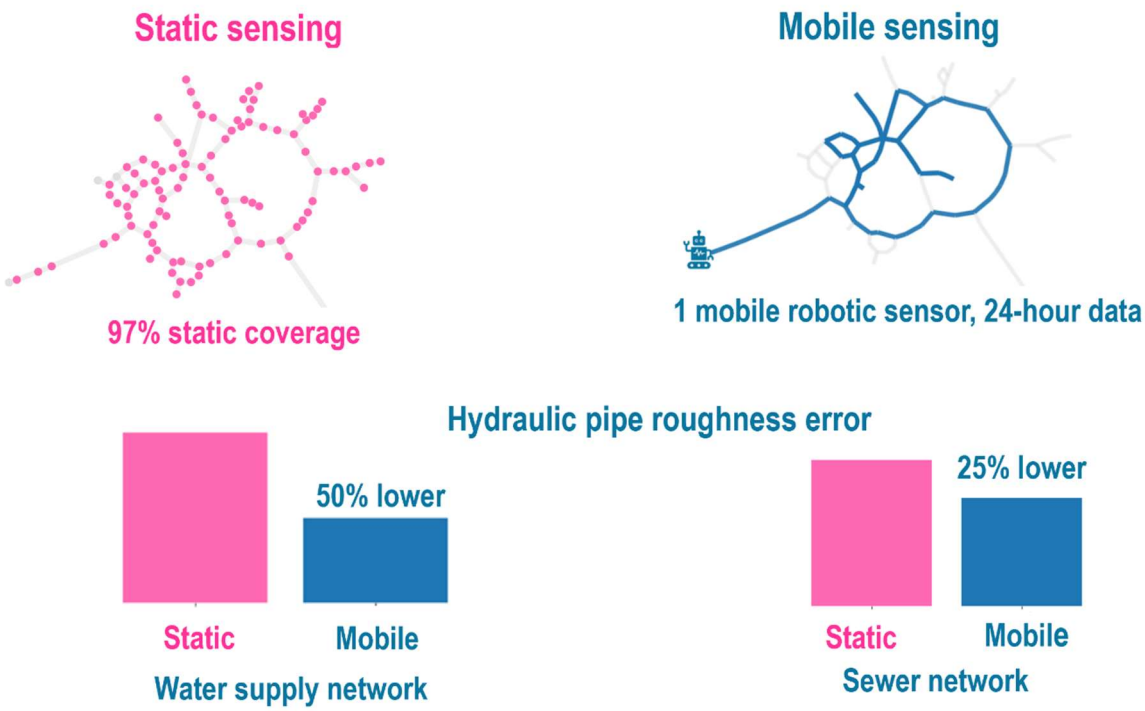

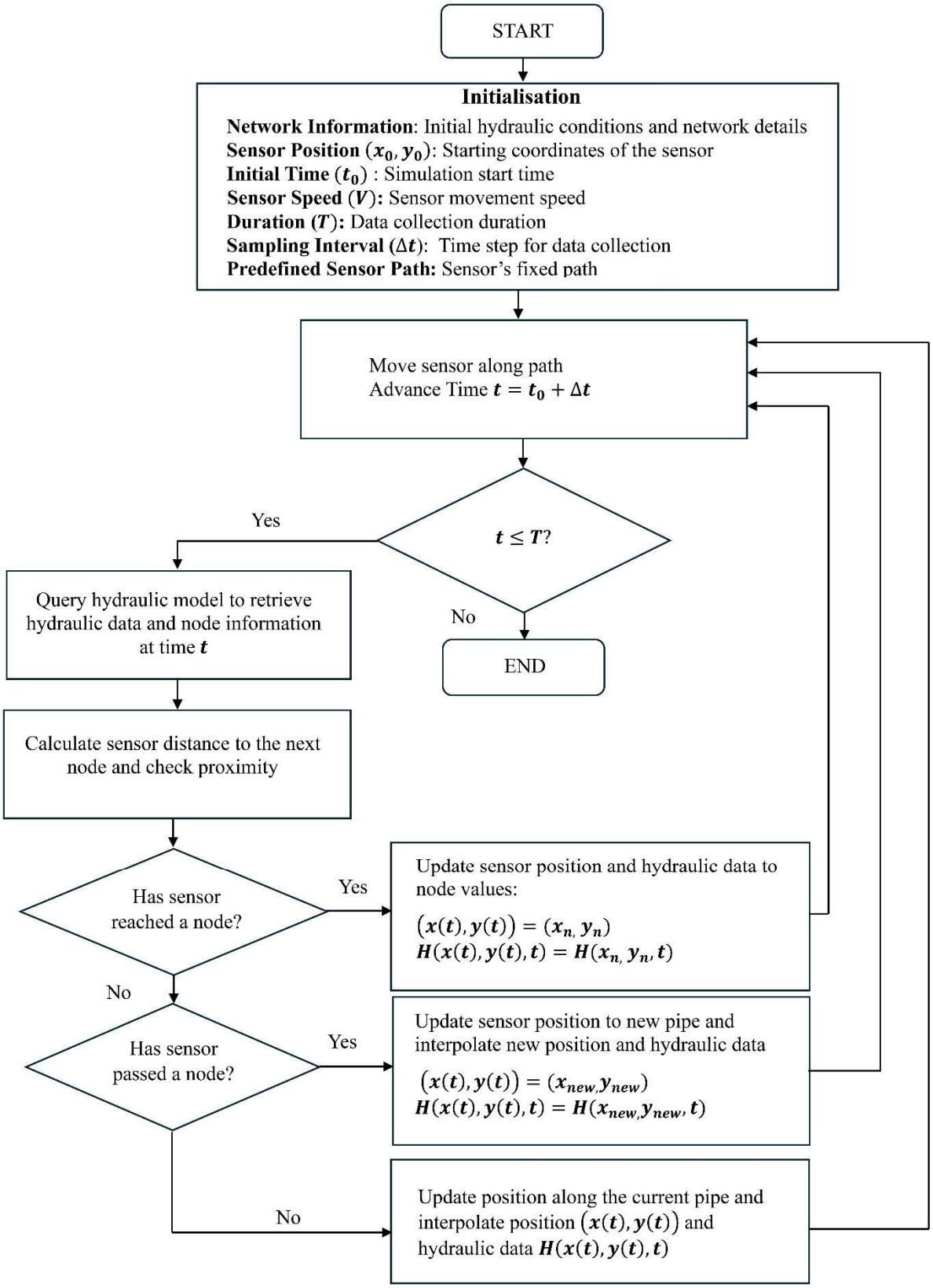

Figure 1. Flowchart of the mobile sensor simulation and hydraulic data collection process. The simulation is executed at each generation of the multi-objective optimisation.

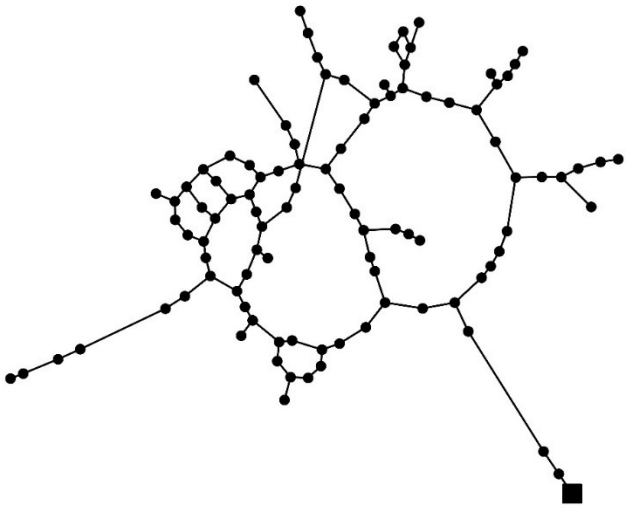

Figure 2. Anonymised Water Supply Network layout for a DMA in the UK.

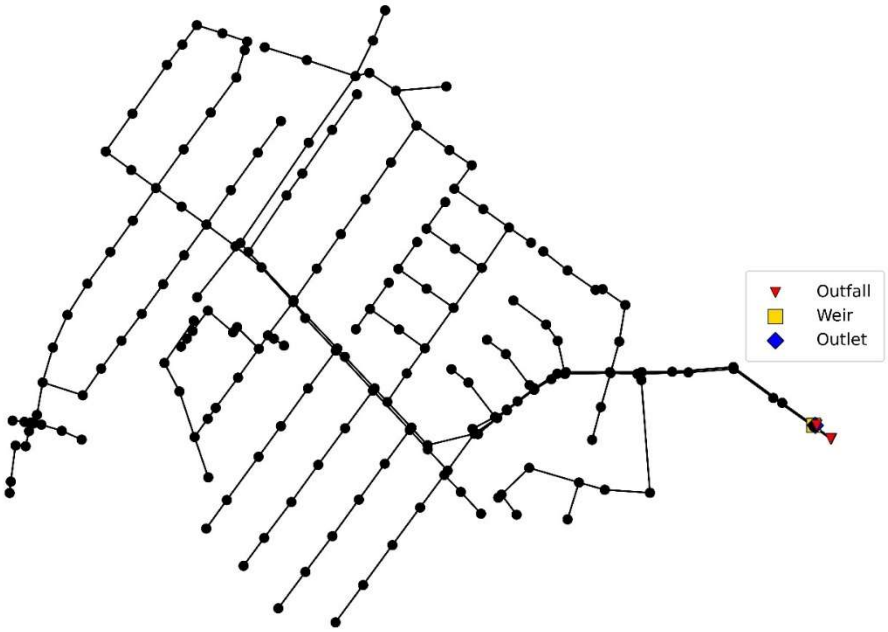

Figure 3. Sewer Network Layout based on Pedersen et al. (2021).

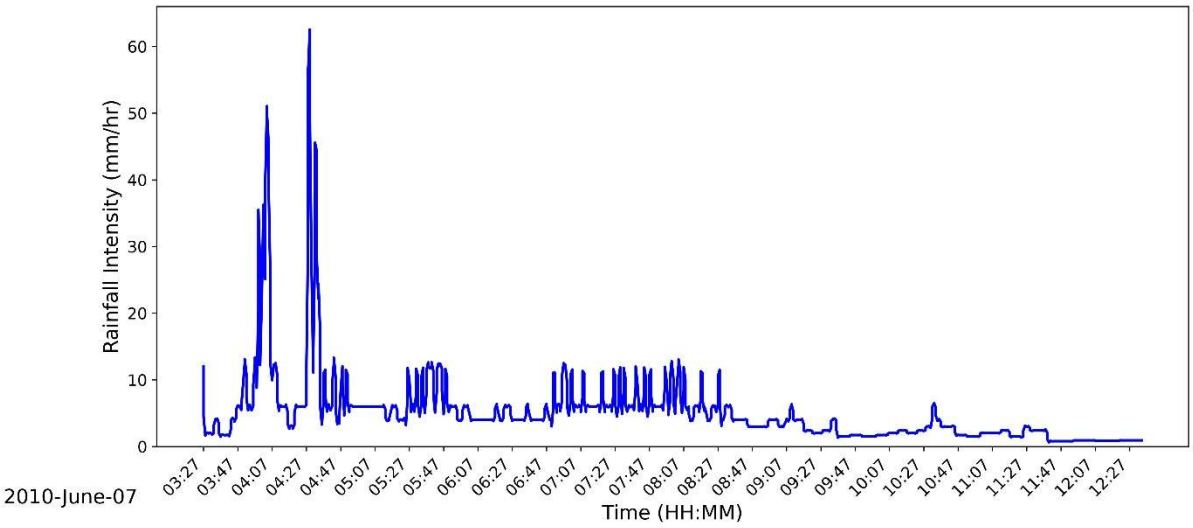

Figure 4. Rainfall intensity versus time plot for the June 7, 2010, event.

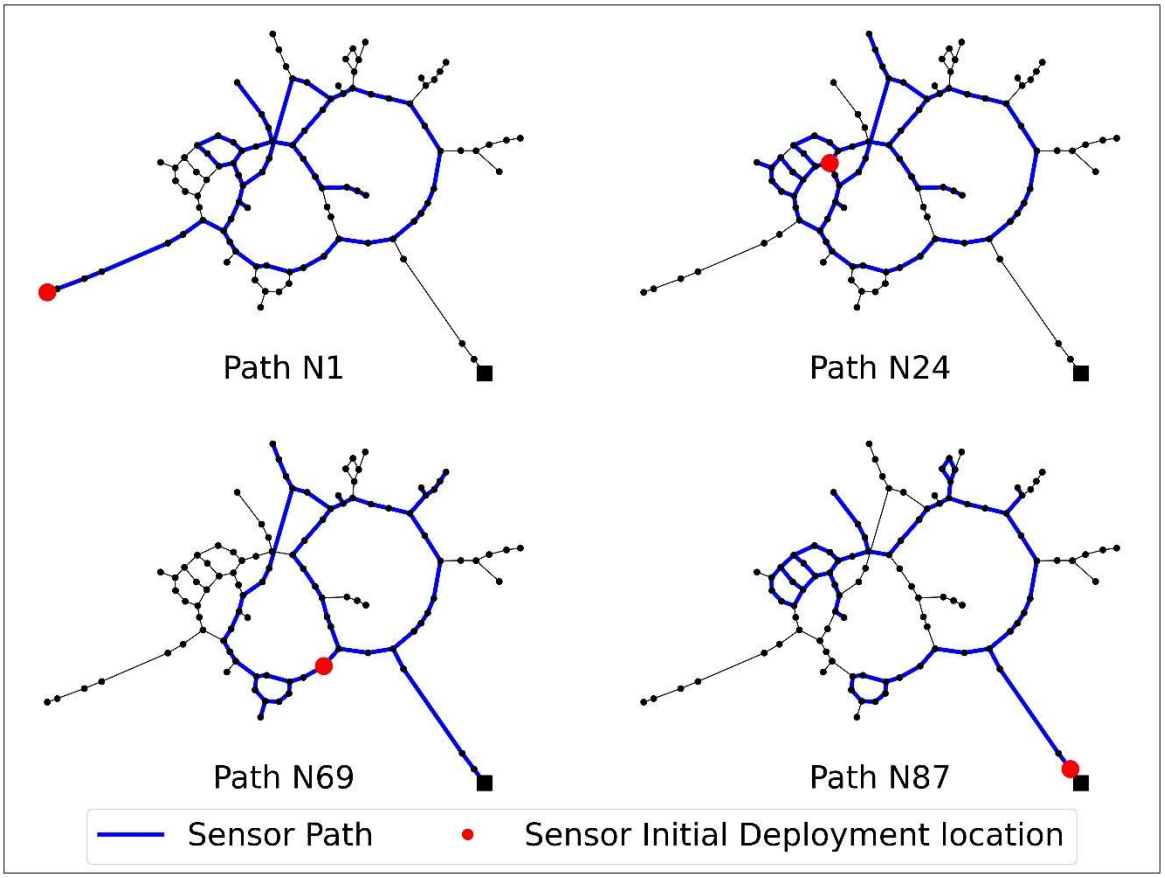

Figure 5. Randomly generated fixed mobile sensor paths originating from four different initial deployment nodes in the water supply network.

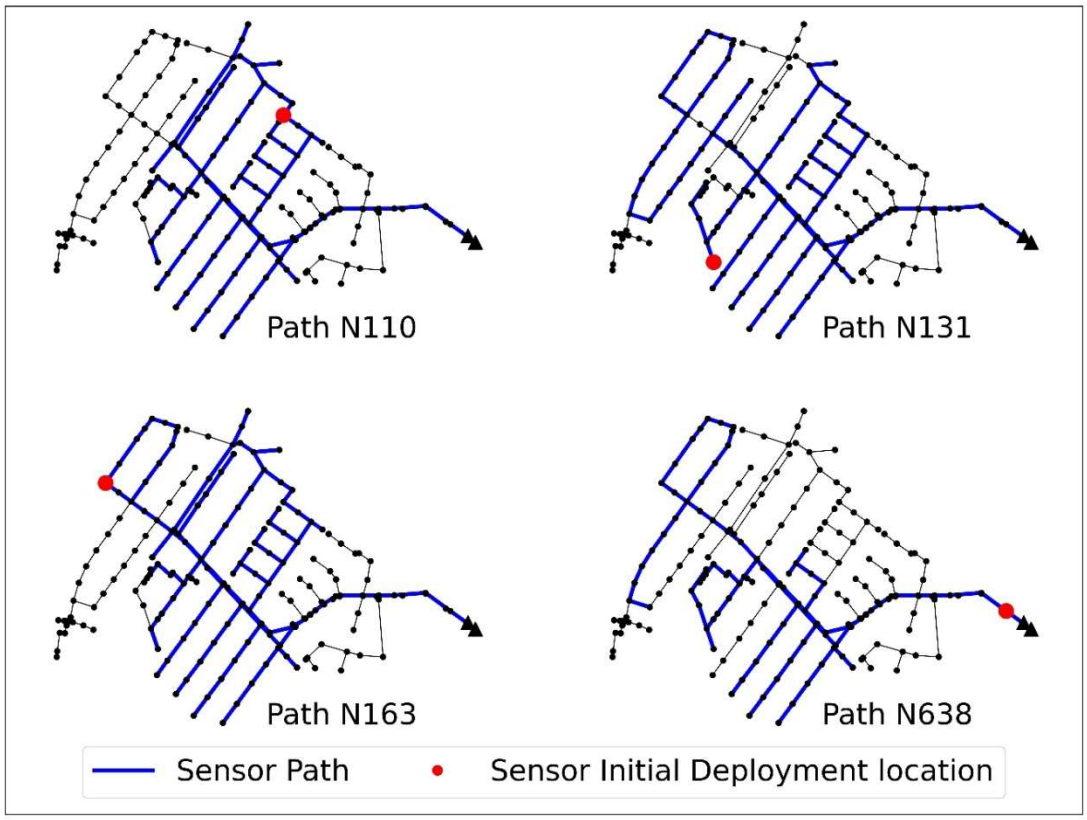

Figure 6. Randomly generated fixed mobile sensor paths originating from four different initial deployment nodes in the sewer network.

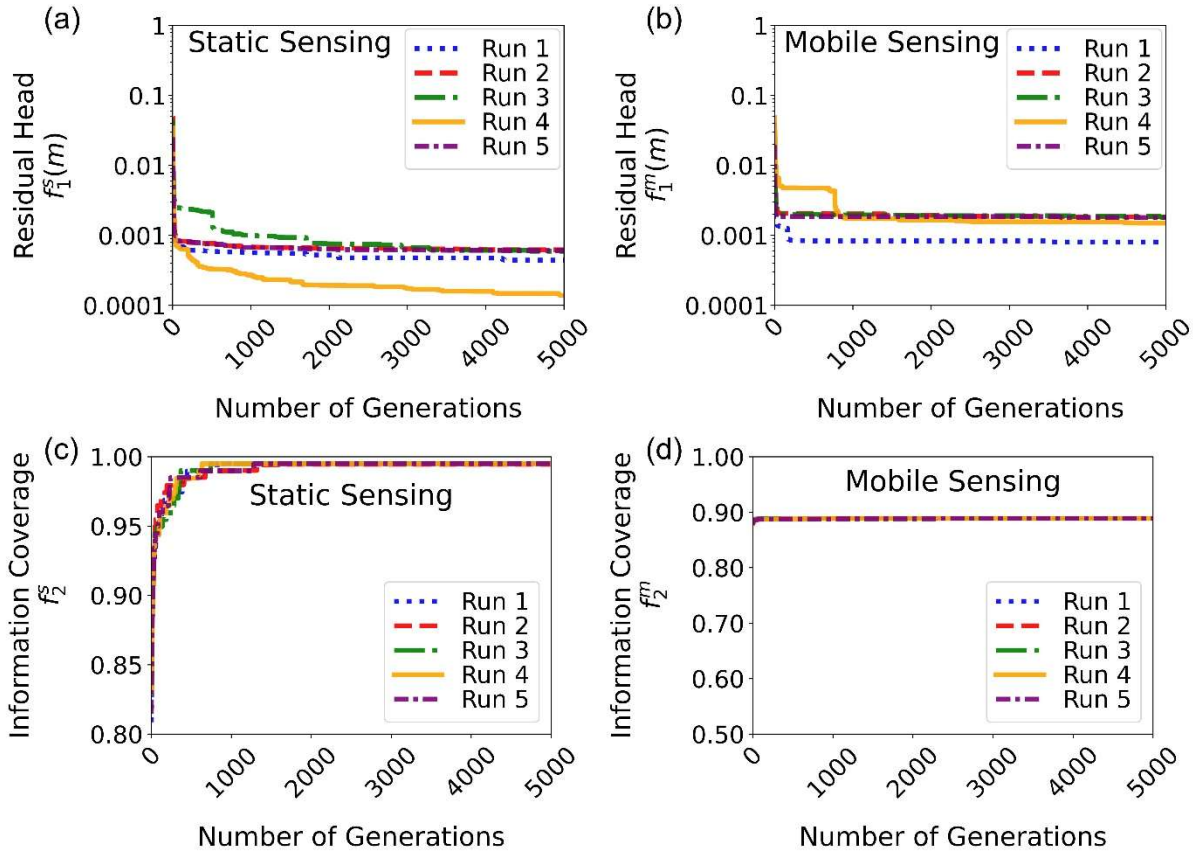

Figure 7. Progression of the residual head (f_1^s and f_1^m) and information coverage (f_2^s and f_2^m) for static and mobile sensing in the water supply network. (a)Progression of f_1^s for static sensing, (b) Progression of f_1^m for mobile sensing path from Node 1, (c) Progression of f_2^s for static sensing, (d) Progression of f_2^m for mobile sensing path from Node 1

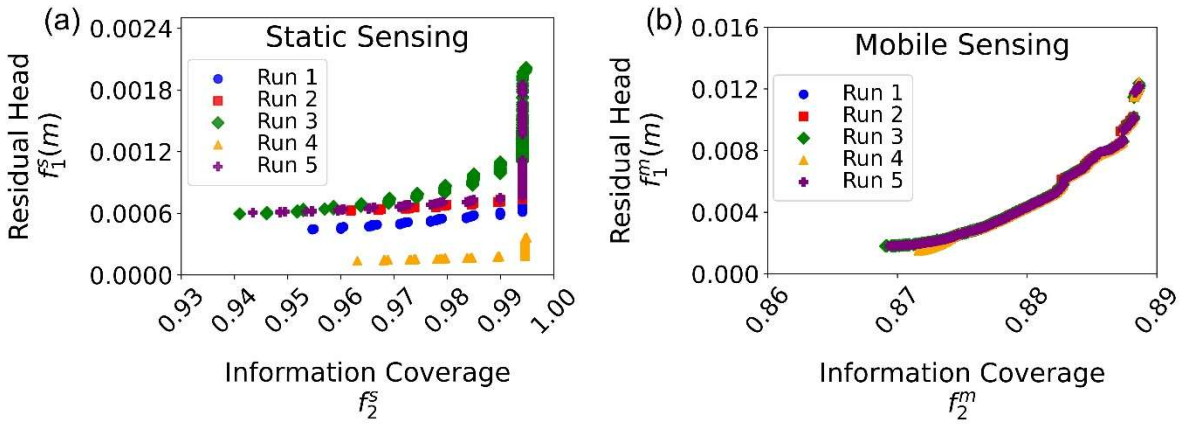

Figure 8. Pareto fronts of the non-dominated solutions at the final generation for the water supply network. Note the Y-axes are not in the same scale. (a) Static sensing, (b) Mobile sensing along Path N1.

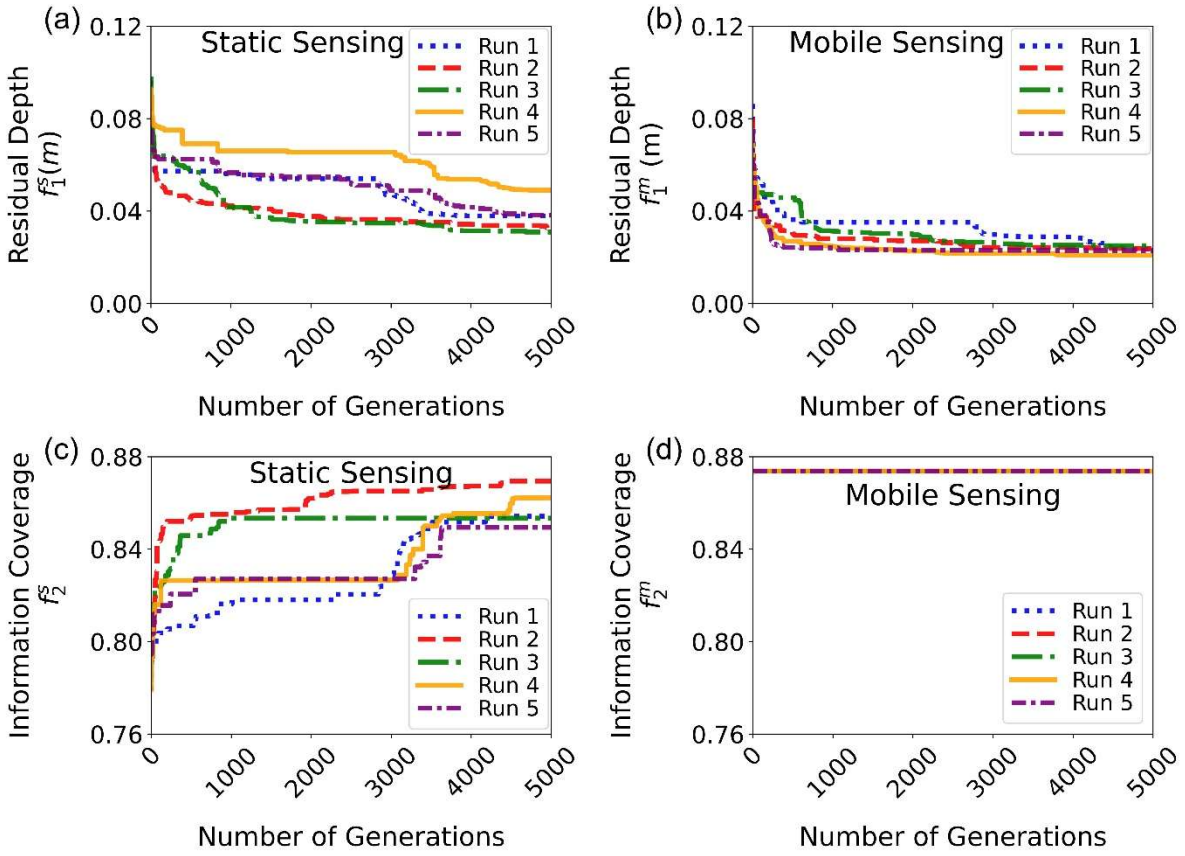

Figure 9. Progression of the residual depth (f_1^s and f_1^m) and information coverage (f_2^s and f_2^m) for static and mobile sensing in the sewer network. (a) Progression of f_1^s for static sensing, (b) Progression of f_1^m for mobile sensing path from Node 638, (c) Progression of f_2^s for static sensing, (d) Progression of f_2^m for mobile sensing path from Node 638.

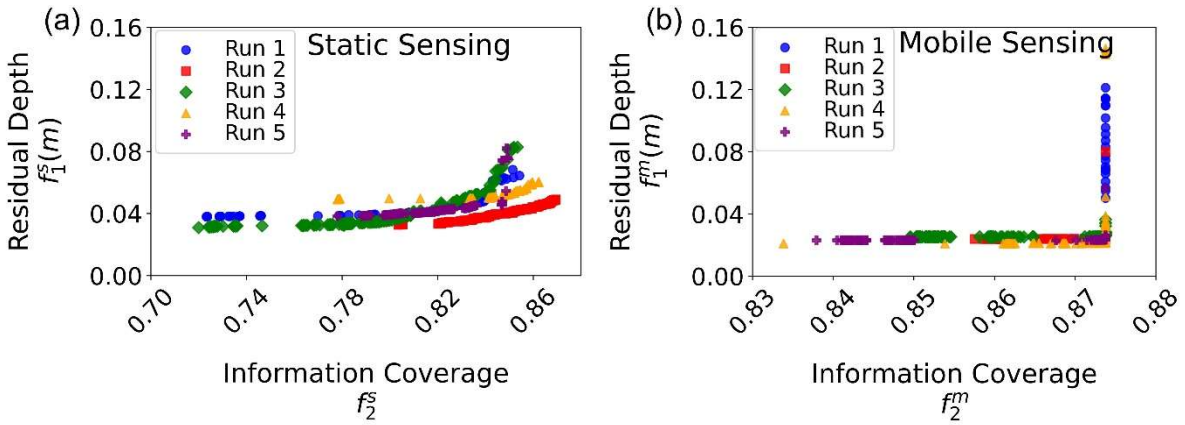

Figure 10. Pareto fronts of the non-dominated solutions at the final generation for the sewer network. (a) Static sensing, (b) Mobile sensing along Path N638.